Variational quantum algorithm for extracing measurments from the Navier-Stokes, Euler and Poisson equations

Pete Rigas, McMahon Lab

November 29, 2020

1 Introduction

The variational quantum algorithm (VQA) has attracted wide attention from several computational disciplines in physics, chemistry and materials science [16], with recent studies demonstrating how optimizers for such algorithms can be improved and parametrized for entanglement [23,24], robust encoding in molecules for chemistry computations [1], various implementations for linear algebra problems [22,26], variance minimization [27], and the construction of quantum Gibbs states [6]. To further contribute to rapid developments, Lubasch et al [15] introduced a VQA which can be applied to solve nonlinear problem from various PDEs through specifications on quantum circuits including an optimized quantum nonlinear processing unit (QNPU) to treat nonlinearities of the equation efficiently, in addition to variational states λ, λ_0 which are prepared in quantum circuits from a cost function $\mathcal{C}(\lambda, \lambda_0)$. In turn, quantum registers prepared in circuits of polynomial depth not only require exponentially fewer parameters than their classical counterparts but also allow for the algorithm to be applied to several other nonlinear problems [15].

To briefly expound upon the algorithm of [15], the algorithm is applied to NLS and the Burger's equation with MPS ansatzae of polynomial bond dimension [19,20]. These particular ansatzae are advantageous for quantum computation in their ability to be represented as a product of isometric matrices, which can be interpreted as the wave function of possible states that are initially imposed on the system through the ansatz before the algorithm is ran to obtain solutions, while also enjoying a two-qubit unitary decomposition that can always be embedded into circuits with polynomial depth. In comparison to cost functions obtained for NLS and the Burger's equations, the Navier-Stokes cost function involves quadratic terms in the magnitude of the time step of the evolution, constant terms directly proportional to the time step and inversely proportional to the Reynolds number, in addition to several other terms resulting from expectation values involving the discretized Nabla and Laplacian operators. We rearrange the cost function in the next section and make use of several identities to obtain expectation terms dependent on the pressure, which under different cases impacts the computation of pressure dependent expectation terms of the cost function. In turn, classical optimization routines will be introduced, in an effort to determine circuit arrangements over which the variational algorithm is capable of generating solutions to the Navier-Stokes equations for different classes of initial data. Modifications to the general requirements imposed on quantum circuits in [15] will be further described.

That is, to apply the hybrid algorithm to study nonlinearities and related behaviors of the Navier-Stokes equations, we optimize the Navier-Stokes cost function for time steps τ in conjunction with running quantum circuit computations given an ansatz. In the following implementation, different numerical aspects of the variational algorithm will be explored through disparate QNPUs, quantum circuits and ansatzae, with qualities of the QNPU construction differing in how nonlinearities of the Navier-Stokes equations are treated; qualities of the quantum circuit construction differing in the number of quantum registers, and hence, variational parameters that need to be specified as the algorithm is executed for solutions; and finally, qualities of ansatzae construction, including the shallow layered ansatz which is comprised of rotation and entangelement operations [17], as well as implications of ansatz construction on the optimization routine of the cost function.

For running the algorithm with nonlinearities besides those which are discussed in [15], it is important to not only determine optimal circuit constructions that reduce noise in gate operations [14,21,31], but also different arrangement of entanglement gates in circuits. Peculiarly, nonlinearities of the Navier-Stokes equations exhibit terms in the cost function which must be computed on entirely different circuit constructions, leading to quantum circuits with readout values from expectations taken between operators denoted $\hat{Q}$, the discretized Nabla and Laplacian about each degree of freedom, and the pressure $\rho(t)$ exerted on the system. To this end, the circuits that will be displayed from terms of the Navier-Stokes cost function are of shallow depth, permitting for comutations over quantum circuits for terms in the Navier-Stokes cost function to be numerically analyzed with Cirq simulations. Notably, the primary difficulties in applying the hybrid variational algorithm to Navier-Stokes is apparent through the QNPU construction for expectation terms from the cost function presented below.

2 Algorithm

2.1 Overview

To quantify time evolution forwards at the initial state and after an increment, we introduce the states Ψ and $\widetilde{\Psi}$. With some abuse of notation, to avoid confusion with the operator $\hat{Q}$ in the cost function we denote the solutions to Navier-Stokes as f. As a result, the Navier-Stokes cost function is of the form,

$$\mathcal{C}(\lambda, \lambda_0) = |\lambda_0|^2 + \left(\frac{\tau}{h}\right)^2 |\tilde{\lambda}_0|^2 + \left(\frac{\tau}{\rho h}\right)^2 + \ 2\ \mathrm{Re}\{-\frac{\tau}{h}\lambda_0^* \tilde{\lambda}_0 \left\langle \Psi | \hat{Q} | \widetilde{\Psi} \right\rangle + \frac{\tau}{\rho h}\lambda_0 \left\langle \Psi | \nabla_x | p \right\rangle - \frac{1}{\rho}\left(\frac{\tau}{h}\right)^2 \tilde{\lambda}_0 \left\langle p | \nabla_x^\dagger \hat{Q} | \widetilde{\Psi} \right\rangle\} \ ,$$

which is readily obtained upon collection of terms from the expansion of $|| \, |f(t+\tau)\rangle - \frac{\tau}{h}\hat{Q} \, |f(t)\rangle + \frac{\tau}{\rho h}\nabla_x \, |p(t)\rangle \, ||^2$ after rearrangement, in which we make use of the straightforward identities for discrete approximations of derivatives in the Navier-Stokes equations after finite differencing, which are,

$$\hat{Q} \, |f(t)\rangle = \langle f(t)| \, \hat{Q}^\dagger \quad \& \quad \nabla_x \, |p(t)\rangle = \langle p(t)| \, \nabla_x^\dagger \ ,$$

by virtue of the expectation being an Hermitian form. Next, the Euler method is applied to obtain $\mathcal{C}$ for variational state preparation, in order to determine ground states in the optimization landscape. From the Navier-Stokes cost function, we identify variational states that are to prepared when the algorithm from [15] is ran. Specifically, the operator $\hat{Q}$ in $\mathcal{C}$ emerges from finite differencing the Navier-Stokes equations and isolating for the time increment of the state of the solution f forwards in time by an increment τ, and takes the form, with $\mathbf{1}$ as the identity operator,

$$\hat{Q} \equiv \frac{h}{\tau}(\mathbf{1} - |f(t)\rangle \, \nabla_x - |v(t)\rangle \, \nabla_y + v\Delta_x + v\Delta_y) \ ,$$

where in $\hat{Q}$ above,

$$\nabla_x = A_x - \mathbf{1} \ , \ \nabla_y = A_y - \mathbf{1} \ ,$$
$$\Delta_x = A_x^\dagger - 2 \times \ \mathbf{1} + A_x \text{ and, } \Delta_y = A_y^\dagger - 2 \times \ \mathbf{1} + A_y \ .$$

We will make use of this procedure to study nonlinearities of the Euler and Poisson equations, in which quantum circuit architecture for computing expectation terms of the cost function above is executed for other PDEs with modifications to the QNPU and CP. After further discussion of the circuit outputs from the variational algorithm for Navier-Stokes, such modifications to the QNPU for the Euler and Poisson equations are valuable for analyzing computational bases with respect to nonlinear behaviors of inviscid flow, amongst other types of time evolution.

From the definition of $\hat{Q}$, we observe that the second and third expectations can be rewritten as,

$$\langle \Psi | \hat{Q} | \widetilde{\Psi} \rangle = \langle \Psi | \left(\frac{h}{\tau}(\mathbf{1} - |f(t)\rangle \, \nabla_x - |v(t)\rangle \, \nabla_y + v\Delta_x + v\Delta_y) \right) | \widetilde{\Psi} \rangle$$
$$= \langle \Psi | \frac{h}{\tau} | \widetilde{\Psi} \rangle + \left(- \langle \Psi | \frac{h}{\tau} \left(\ |f(t)\rangle \ \right) | \widetilde{\Psi} \rangle \right) + \left(- \langle \Psi | \frac{h}{\tau} \left(\ |v(t)\rangle \ \right) | \widetilde{\Psi} \rangle \right) + \langle \Psi | \frac{h}{\tau} \left(v\Delta_x \right) | \widetilde{\Psi} \rangle + \langle \Psi | \frac{h}{\tau} \left(v\Delta_y \right) | \widetilde{\Psi} \rangle$$
$$= \frac{h}{\tau} \Bigg(\langle \Psi | \mathbf{1} | \widetilde{\Psi} \rangle + \left(- \langle \Psi | \left(\ |f(t)\rangle \ \right) | \widetilde{\Psi} \rangle \right) + \left(- \langle \Psi | \left(\ |v(t)\rangle \ \right) | \widetilde{\Psi} \rangle \right) + \langle \Psi | v\Delta_x | \widetilde{\Psi} \rangle +$$
$$\langle \Psi | v\Delta_y | \widetilde{\Psi} \rangle \Bigg) \ ,$$

which amounts to computing the summation of expectations above, with the final resultant multiplied by $\frac{h}{\tau}$ corresponding to the second term. As for the third term, we can similarly expand by making use of the definition of $\hat{Q}$, obtaining

$$\langle p|\nabla_x^\dagger \hat{Q}|\widetilde{\Psi}\rangle = \langle p|\nabla_x^\dagger\bigg(\frac{h}{\tau}(\mathbf{1} - |f(t)\rangle\,\nabla_x - |v(t)\rangle\,\nabla_y + v\Delta_x + v\Delta_y)\bigg)|\widetilde{\Psi}\rangle$$
$$= \langle p|\frac{h}{\tau}\bigg(\nabla_x^\dagger\bigg)|\widetilde{\Psi}\rangle + \bigg(-\langle p|\frac{h}{\tau}\nabla_x^\dagger\bigg(\,|f(t)\rangle\bigg)\nabla_x|\widetilde{\Psi}\rangle\bigg) + \bigg(-\langle p|\frac{h}{\tau}\nabla_x^\dagger\bigg(\,|v(t)\rangle\bigg)\nabla_y|\widetilde{\Psi}\rangle\bigg) + \langle p|\frac{hv\Delta_x}{\tau}|\widetilde{\Psi}\rangle$$
$$+ \langle p|\frac{hv\Delta_y}{\tau}|\widetilde{\Psi}\rangle$$
$$= \frac{h}{\tau}\bigg(\,\langle p|\bigg(\nabla_x^\dagger\bigg)|\widetilde{\Psi}\rangle + \bigg(-\langle p|\nabla_x^\dagger\bigg(\,|f(t)\rangle\bigg)\nabla_x|\widetilde{\Psi}\rangle\bigg) + \bigg(-\langle p|\nabla_x^\dagger\bigg(\,|v(t)\rangle\bigg)\nabla_y|\widetilde{\Psi}\rangle\bigg) + \langle p|v\Delta_x|\widetilde{\Psi}\rangle$$
$$+ \langle p|v\Delta_y|\widetilde{\Psi}\rangle\bigg)\,,$$

allowing for further rearrangements from respective collection of like terms in $|v(t)\rangle$, $|f(t)\rangle$, $v\Delta_x$ and $v\Delta_y$, between the second and third expectation terms, giving

$$\frac{h}{\tau}\bigg(-\langle p|\bigg(\,|v(t)\rangle + \nabla_x^\dagger\,|v(t)\rangle\,\nabla_x\bigg)|\widetilde{\Psi}\rangle\bigg)\,,$$

for $|v(t)\rangle$, while

$$\frac{h}{\tau}\bigg(-\langle p|\bigg(\,|f(t)\rangle + \nabla_x^\dagger\,|f(t)\rangle\,\nabla_x\bigg)|\widetilde{\Psi}\rangle\bigg)\,,$$

for $|f(t)\rangle$. Also, the remaining two terms dependent on v take the form,

$$\frac{2h}{\tau}\bigg(\,\langle p|v\Delta_x|\tilde{\Psi}\rangle + \langle\Psi|v\Delta_y|\tilde{\Psi}\rangle\bigg)\,.$$

Hence applying linearity of expectation where appropriate in turn gives a cost function of the form, through the superposition

$$|\lambda_0|^2 + \bigg(\frac{\tau}{h}\bigg)^2|\tilde{\lambda}_0|^2 + \bigg(\frac{\tau}{\rho h}\bigg)^2 + \;\frac{2\;h}{\tau}\;\mathrm{Re}\;\{\;\langle\Psi|\mathbf{1}|\widetilde{\Psi}\rangle + \langle p|\bigg(\nabla_x^\dagger\bigg)|\widetilde{\Psi}\rangle - \langle\Psi|\bigg(\,|v(t)\rangle\bigg)|\widetilde{\Psi}\rangle + \langle p|\nabla_x^\dagger\,|v(t)\rangle\,\nabla_x|\widetilde{\Psi}\rangle -$$
$$\langle p|\bigg(\,|f(t)\rangle + \nabla_x^\dagger\,|f(t)\rangle\,\nabla_x\bigg)|\widetilde{\Psi}\rangle + \;2\bigg(\,\langle p|v\Delta_x|\widetilde{\Psi}\rangle + \langle\Psi|v\Delta_y|\widetilde{\Psi}\rangle\bigg)\;\}\;,$$

which can be rearranged more explicitly, through substitution in terms with ∇_x, ∇_y, Δ_x and Δ_y, for the second term taken under Re,

$$\langle p|\bigg(\nabla_x^\dagger\bigg)|\widetilde{\Psi}\rangle = \langle p|\bigg(A_x^\dagger - \mathbf{1}\bigg)|\widetilde{\Psi}\rangle\;\;,$$

and similarly for the third and fourth terms taken under Re,

$$\langle\Psi|\bigg(\,|v(t)\rangle\bigg)|\widetilde{\Psi}\rangle + \langle p|\nabla_x^\dagger\,|v(t)\rangle\,\nabla_x|\widetilde{\Psi}\rangle = \langle\Psi|\bigg(\,|v(t)\rangle\bigg)|\widetilde{\Psi}\rangle + \langle p|\bigg(\{A_x^\dagger - \mathbf{1}\}\,|v(t)\rangle\,\{A_x - \mathbf{1}\}\bigg)|\widetilde{\Psi}\rangle\;\;.$$

For the fourth term taken under Re, we get

$$\langle p|\Big(\,|f(t)\rangle + \nabla_x^\dagger\,|f(t)\rangle\,\nabla_x\Big)|\widetilde{\Psi}\rangle = \langle p|\Big(\,|f(t)\rangle + \{A_x^\dagger - \mathbf{1}\}\,|f(t)\rangle\,\{A_x - \mathbf{1}\}\Big)|\widetilde{\Psi}\rangle \;\;,$$

and finally from the fourth term multiplied by 2,

$$\langle p|v\Delta_x|\widetilde{\Psi}\rangle + \langle\Psi|v\Delta_y|\widetilde{\Psi}\rangle = \langle p|v\Big(A_x^\dagger - 2\times\;\mathbf{1} + A_x\Big)|\tilde{\Psi}\rangle + \langle\Psi|v\Big(A_y^\dagger - 2\times\;\mathbf{1} + A_y\Big)|\widetilde{\Psi}\rangle \;\;,$$

from which we collect all rearrangements, in turn obtaining a cost function of the form from like terms,

$$\begin{aligned}|\lambda_0|^2 + \Big(\frac{\tau}{h}\Big)^2|\tilde{\lambda}_0|^2 + \Big(\frac{\tau}{\rho h}\Big)^2 + \;\frac{2\,h}{\tau}\;\mathrm{Re}\;\{\;\langle\Psi|\mathbf{1}|\widetilde{\Psi}\rangle + \langle p|\Big(A_x^\dagger - \mathbf{1}\Big)|\widetilde{\Psi}\rangle + \langle\Psi|\Big(\,|v(t)\rangle\Big)\;\widetilde{\Psi}\rangle \;\;-\\ \langle p|\Big(\{A_x^\dagger - \mathbf{1}\}\,|v(t)\rangle\,\{A_x - \mathbf{1}\}\Big)|\widetilde{\Psi}\rangle - \langle p|\Big(\,|f(t)\rangle + \{A_x^\dagger - \mathbf{1}\}\,|f(t)\rangle\,\{A_x - \mathbf{1}\}\Big)|\widetilde{\Psi}\rangle + \\ 2\Big(\,\langle p|v\Big(A_x^\dagger - 2\times\;\mathbf{1} + A_x\Big)|\tilde{\Psi}\rangle + \langle\Psi|v\Big(A_y^\dagger - 2\times\;\mathbf{1} + A_y\Big)|\widetilde{\Psi}\rangle\Big)\}\;,\end{aligned}$$

from which rearranging fifth expectation term under Re gives, by making use of the identity $|f(t)\rangle = \lambda_0\,|\Psi\rangle$, which is related to the time evolved quantum state which satisfies $|f(t+\tau)\rangle = \widetilde{\lambda}_0\,|\widetilde{\Psi}\rangle$ for variational states,

$$\begin{aligned}\langle p|\Big(\{\tilde{\lambda}_0\,|\widetilde{\Psi}\rangle\} + \{A_x^\dagger - \mathbf{1}\}\{\tilde{\lambda}_0\,|\widetilde{\Psi}\rangle\}\{A_x - \mathbf{1}\}\Big)|\widetilde{\Psi}\rangle &= \Big(\,\langle p|\,\{\widetilde{\lambda}_0\,|\widetilde{\Psi}\rangle\} + \langle p|\,\{A_x^\dagger - \mathbf{1}\}\{\widetilde{\lambda}_0\,|\widetilde{\Psi}\rangle\}(A_x - \mathbf{1})\Big)\,|\widetilde{\Psi}\rangle \;\;,\\ &= \langle p|\{\tilde{\lambda}_0\,|\widetilde{\Psi}\rangle|\widetilde{\Psi}\rangle + \langle p|\{A_x^\dagger - \mathbf{1}\}\{\widetilde{\lambda}_0\,|\widetilde{\Psi}\rangle\}(A_x - \mathbf{1})|\widetilde{\Psi}\rangle \;\;,\end{aligned}$$

which yields the desired cost function for Navier-Stokes below after substituting in for variational states for the solution to the Navier-Stokes equations, yielding,

$$\begin{aligned}\boxed{\mathcal{C}^x(\lambda,\lambda_0)} = |\lambda_0|^2 + \Big(\frac{\tau}{h}\Big)^2|\tilde{\lambda}_0|^2 + \Big(\frac{\tau}{\rho h}\Big)^2 + \;\frac{2\,h}{\tau}\;\mathrm{Re}\;\{\;\langle\Psi|\mathbf{1}|\widetilde{\Psi}\rangle + \langle p|\Big(A_x^\dagger - \mathbf{1}\Big)|\widetilde{\Psi}\rangle + \langle\Psi|\Big(\,|v(t)\rangle\Big)\;\widetilde{\Psi}\rangle \;\;-\\ \langle p|\Big(\{A_x^\dagger - \mathbf{1}\}\,|v(t)\rangle\,\{A_x - \mathbf{1}\}\Big)|\widetilde{\Psi}\rangle - \langle p|\{\tilde{\lambda}_0\,|\widetilde{\Psi}\rangle|\widetilde{\Psi}\rangle - \langle p|\{A_x^\dagger - \mathbf{1}\}\{\widetilde{\lambda}_0\,|\widetilde{\Psi}\rangle\}(A_x - \mathbf{1})|\widetilde{\Psi}\rangle \;\;+\\ 2\Big(\,\langle p|v\Big(A_x^\dagger - 2\times\;\mathbf{1} + A_x\Big)|\tilde{\Psi}\rangle + \langle\Psi|v\Big(A_y^\dagger - 2\times\;\mathbf{1} + A_y\Big)|\widetilde{\Psi}\rangle\Big)\}\;,\end{aligned}\qquad (\bigstar)$$

for the x component of the solution.

As one modification to the Lubasch et al variational algorithm, another cost function must be introduced within the QNPU which has expectation terms dependent on the other component of the solution which appears in the Navier-Stokes equations. We denote this additional cost function as $\mathcal{C}^y(\lambda,\lambda_0)$. The circuit diagram provided in *Figure 2* illustrates the expectation terms from this cost function for only one component of the solution. Due to the no-cloning theorem, to accommodate expectation terms associated with the remaining cost function $\mathcal{C}^y$ for the remaining component of the solution, we must prepare additional states outside of those illustrated in the ancillary registers of *Figure 1.*

Within $\mathcal{C}$, it is necessary that we introduce cost functions for $|v(t)\rangle$ so that corresponding quantum states to each quantity can be stored appropriately on registers in the quantum computer. To do this, we follow similar procedures used to obtain the first Navier-Stokes cost function, as we formulate cost functions which correspond to different classes of pressure distributions. [1]

To this end, we introduce several cases to further study the computations associated with different pressure dependent expectation terms from the Navier-Stokes cost function. If the pressure distribution is uniform, in the simplest case each

[1]Further remarks will also shed light upon determining ground states for the Navier-Stokes cost function in a constant pressure distribution which remains constant with time steps in the evolution.

pressure dependent term amounts to the expectation with a quantity that is uniformly distributed over the domain. In more realistic cases, the variational state $|p(t+\tau)\rangle$ after $|p(t)\rangle$ is time evolved forwards requiries specification of additional variational parameters λ^p, in addition to an accompanying unitary operator as the time evolution is computed. We introduce classes of admissible pressure distributions for the Navier-Stokes equations in the following cases. The expectation terms from $\mathcal{C}^x$ and $\mathcal{C}^y$ which will be impacted are indicated in orange. In the cases below, we discuss how the pressure distribution would be prepared and computed on the quantum computer for one coordinate, from which computations for the remaining component easily follow.

We make use of previous rearrangements after substituting in $\hat{Q}$ and prepare corresponding variational states of the pressure distribution p after time evolution, which are readily obtained from ★. From previous studies of exact solutions to Navier-Stokes [32], pressure distributions corresponding to solutions in the plane focus on analyses of convective terms under which solutions are known to exist. Below, we gather results by reading off expectation terms from the Navier-Stokes cost function which are dependent on the pressure, and afterwards identifying admissible pressure distributions from solutions to the equations presented in the literature, in addition to additional formulations of the cost function.

2.1.1 Vanishing pressure distribution

Under a pressure distribution with no magnitude at every point on the domain over which readout for Navier-Stokes is produced, the cost function simplifies to the following. We simply cross off terms if one term in the expectation vanishes, in which

$$\boxed{\mathcal{C}^{\,0,x}(\lambda,\lambda_0)} = |\lambda_0|^2 + \left(\frac{\tau}{h}\right)^2 |\tilde{\lambda}_0|^2 + \left(\frac{\tau}{\rho h}\right)^2 + \frac{2\,h}{\tau}\,\mathrm{Re}\,\{\ \langle\Psi|\mathbf{1}|\widetilde{\Psi}\rangle + \langle\Psi|\Big(\ |v(t)\rangle\Big)\ \widetilde{\Psi}\rangle\ - 2\Big(\ \langle\Psi|v\Big(A_y^\dagger - 2\times\ \mathbf{1} + A_y\Big)|\widetilde{\Psi}\rangle\ \Big)\}\ ,$$

for the cost function of the x component of the solution under no pressure distribution.

In the remaining cases, the following cost functions differ in pressure dependent expectation terms from ★ in orange.

2.1.2 Uniform pressure distribution

For a uniform distribution $\mathcal{U}$ the time evolution of the pressure for any time step remains unchanged. Simply, the most nontrivial cost function for the magnitude of the pressure over each grid point of the discretization yields the following, when $p \equiv c$ with $c > 0$,

$$\boxed{\mathcal{C}^{\,\mathcal{U},x}(\lambda,\lambda_0)} = |\lambda_0|^2 + \left(\frac{\tau}{h}\right)^2 |\tilde{\lambda}_0|^2 + \left(\frac{\tau}{\rho h}\right)^2 + \frac{2\,h}{\tau}\,\mathrm{Re}\,\{\ \langle\Psi|\mathbf{1}|\widetilde{\Psi}\rangle + \langle c|\Big(A_x^\dagger - \mathbf{1}\Big)|\widetilde{\Psi}\rangle + \langle\Psi|\Big(\ |v(t)\rangle\Big)\ \widetilde{\Psi}\rangle\ - \langle c|\Big(\{A_x^\dagger - \mathbf{1}\}\,|v(t)\rangle\,\{A_x - \mathbf{1}\}\Big)|\widetilde{\Psi}\rangle - \langle c|\{\tilde{\lambda}_0\,|\widetilde{\Psi}\rangle|\widetilde{\Psi}\rangle - \langle c|\{A_x^\dagger - \mathbf{1}\}\{\tilde{\lambda}_0\,|\widetilde{\Psi}\rangle\}(A_x - \mathbf{1})|\widetilde{\Psi}\rangle\ + 2\Big(\ \langle c|v\Big(A_x^\dagger - 2\times\ \mathbf{1} + A_x\Big)|\widetilde{\Psi}\rangle + \langle\Psi|v\Big(A_y^\dagger - 2\times\ \mathbf{1} + A_y\Big)|\widetilde{\Psi}\rangle\ \Big)\}\ ,$$

through modifications to the expectation terms from $\mathcal{C}$ which are dependent on p, in orange. In comparison with the most simple pressure distribution assumption in the previous case, $\mathcal{C}^{\,\mathcal{U},x}$ retains all pressure dependent expectation terms.

2.1.3 Linearly dependent $\mathcal{L}$ pressure distribution

With respect to the location in the optimization landscape

In relevant expectation terms, a pressure distribution which varies linearly with respect to space yields the following superposition, including pressure dependent expectation terms,

$$\boxed{\mathcal{C}^{\mathcal{L},x}(\lambda,\lambda_0)} = |\lambda_0|^2 + \left(\frac{\tau}{h}\right)^2 |\tilde{\lambda}_0|^2 + \left(\frac{\tau}{\rho h}\right)^2 + \frac{2\,h}{\tau}\,\mathrm{Re}\,\{\ \langle\Psi|\mathbf{1}|\widetilde{\Psi}\rangle + \langle\mathcal{L}|\Big(A_x^\dagger - \mathbf{1}\Big)|\widetilde{\Psi}\rangle + \langle\Psi|\Big(\,|v(t)\rangle\,\Big)\,\widetilde{\Psi}\rangle\ -$$
$$\langle\mathcal{L}|\Big(\{A_x^\dagger - \mathbf{1}\}\,|v(t)\rangle\,\{A_x - \mathbf{1}\}\Big)|\widetilde{\Psi}\rangle - \langle\mathcal{L}|\{\widetilde{\lambda}_0\,|\widetilde{\Psi}\rangle|\widetilde{\Psi}\rangle - \langle\mathcal{L}|\{A_x^\dagger - \mathbf{1}\}\{\widetilde{\lambda}_0\,|\widetilde{\Psi}\rangle\}(A_x - \mathbf{1})|\widetilde{\Psi}\rangle\ +$$
$$2\Big(\,\langle\mathcal{L}|v\Big(A_x^\dagger - 2\times\ \mathbf{1} + A_x\Big)|\tilde{\Psi}\rangle + \langle\Psi|v\Big(A_y^\dagger - 2\times\ \mathbf{1} + A_y\Big)|\widetilde{\Psi}\rangle\,\Big)\}\ ,$$

which results in the following modification to the circuit architecture discussed in the next section, and displayed in *Figure 1 & Figure 2*. Specifically, if the pressure distribution is proportional to the absolute value of the coordinate of space at which the sample is drawn, then additional ancillary registers in the circuit must be prepared so as to keep track of the location at which the sample is gathered rather than its magnitude alone. Such a class of distributions is realistic for further complexity upon the distribution assumption in the previous two cases. Performing simple manipulations under this assumption gives, respectively for the second, fourth, fifth, sixth, and seventh terms under Re,

$$\boxed{2} \Rightarrow \langle\mathcal{L}|\Big(A_x^\dagger - \mathbf{1}\Big)|\widetilde{\Psi}\rangle = \Big(\,\langle\mathcal{L}|\,\Big(A_x^\dagger - \mathbf{1}\Big)\Big)\,|\widetilde{\Psi}\rangle = \Big(\,\langle\mathcal{L}|\,A_x^\dagger - \langle\mathcal{L}|\,\mathbf{1}\,\Big)\,|\widetilde{\Psi}\rangle = \langle\mathcal{L}|A_x^\dagger|\widetilde{\Psi}\rangle - \langle\mathcal{L}|\mathbf{1}|\widetilde{\Psi}\rangle\ ,$$

$$\boxed{4} \Rightarrow \langle\mathcal{L}|\Big(\{A_x^\dagger - \mathbf{1}\}\,|v(t)\rangle\,\{A_x - \mathbf{1}\}\Big)|\widetilde{\Psi}\rangle = \Big(\,\langle\mathcal{L}|\,\Big(\{A_x^\dagger - \mathbf{1}\}\,|v(t)\rangle\,\{A_x - \mathbf{1}\}\Big)\Big)\,|\widetilde{\Psi}\rangle = \langle\mathcal{L}|\,\Big(\{A_x^\dagger - \mathbf{1}\}\,|v(t)\rangle\,\{A_x - \mathbf{1}\}\Big)\,|\widetilde{\Psi}\rangle =$$
$$\Big(\Big(\,\langle\mathcal{L}|\{A_x^\dagger - \mathbf{1}\}|v(t)\rangle\,\Big)\{A_x - \mathbf{1}\}\Big)\,|\widetilde{\Psi}\rangle\ ,$$

$$\boxed{5} \Rightarrow \langle\mathcal{L}|\{\widetilde{\lambda}_0\,|\widetilde{\Psi}\rangle\}|\widetilde{\Psi}\rangle = \Big(\,\langle\mathcal{L}|\,\{\widetilde{\lambda}_0\,|\widetilde{\Psi}\rangle\}\Big)\,|\widetilde{\Psi}\rangle = \Big(\,\langle\mathcal{L}|\widetilde{\lambda}_0|\widetilde{\Psi}\rangle\,\Big)\,|\widetilde{\Psi}\rangle$$

$$\boxed{6} \Rightarrow \langle\mathcal{L}|\{A_x^\dagger - \mathbf{1}\}\{\widetilde{\lambda}_0\,|\widetilde{\Psi}\rangle\}(A_x - \mathbf{1})|\widetilde{\Psi}\rangle = \langle\mathcal{L}|\,\Big(\{A_x^\dagger - \mathbf{1}\}\{\widetilde{\lambda}_0\,|\widetilde{\Psi}\rangle\}(A_x - \mathbf{1})\Big)\,|\widetilde{\Psi}\rangle = \Big(\,\langle\mathcal{L}|\Big(A_x^\dagger\widetilde{\lambda}_0 - \widetilde{\lambda}_0\Big)|\widetilde{\Psi}\rangle\,(A_x - \mathbf{1})\Big)\,|\widetilde{\Psi}\rangle =$$
$$\Big(\{\langle\mathcal{L}|\Big(A_x^\dagger\widetilde{\lambda}_0 - \widetilde{\lambda}_0\Big)\}|\widetilde{\Psi}\rangle\Big)(A_x - \mathbf{1})\,|\widetilde{\Psi}\rangle\ ,$$

$$\boxed{7} \Rightarrow \langle\mathcal{L}|v\Big(A_x^\dagger - 2\times\ \mathbf{1} + A_x\Big)|\tilde{\Psi}\rangle = \langle\mathcal{L}|\Big(vA_x^\dagger - 2\times v + vA_x\Big)|\widetilde{\Psi}\rangle =$$
$$\langle\mathcal{L}|vA_x^\dagger|\widetilde{\Psi}\rangle - \langle\mathcal{L}|\{2\times v\}|\widetilde{\Psi}\rangle + \langle\mathcal{L}|vA_x|\widetilde{\Psi}\rangle =$$
$$\langle\mathcal{L}|vA_x^\dagger|\widetilde{\Psi}\rangle - 2\,\langle\mathcal{L}|v|\widetilde{\Psi}\rangle + \langle\mathcal{L}|vA_x|\widetilde{\Psi}\rangle\ .$$

Finally, collecting all terms in $\mathcal{C}^{\,\mathcal{L},x}$ in light of such rearrangements gives,

$$\boxed{\mathcal{C}^{\mathcal{L},x}(\lambda,\lambda_0)} = |\lambda_0|^2 + \left(\frac{\tau}{h}\right)^2 |\tilde{\lambda}_0|^2 + \left(\frac{\tau}{\rho h}\right)^2 + \frac{2\,h}{\tau}\,\mathrm{Re}\,\{\ \langle\Psi|\mathbf{1}|\widetilde{\Psi}\rangle\ +\ \overbrace{\langle\mathcal{L}|A_x^\dagger|\widetilde{\Psi}\rangle - \langle\mathcal{L}|\mathbf{1}|\widetilde{\Psi}\rangle}^{\boxed{2}}\ +$$
$$\langle\Psi|\Big(\,|v(t)\rangle\,\Big)\,\widetilde{\Psi}\rangle\ -\ \overbrace{\Big(\Big(\,\langle\mathcal{L}|\{A_x^\dagger - \mathbf{1}\}|v(t)\rangle\,\Big)\{A_x - \mathbf{1}\}\Big)\,|\widetilde{\Psi}\rangle}^{\boxed{4}} - \overbrace{\Big(\,\langle\mathcal{L}|\widetilde{\lambda}_0|\widetilde{\Psi}\rangle\,\Big)\,|\widetilde{\Psi}\rangle}^{\boxed{5}}\ -$$
$$\overbrace{\Big(\{\langle\mathcal{L}|\Big(A_x^\dagger\widetilde{\lambda}_0 - \widetilde{\lambda}_0\Big)\}\,|\widetilde{\Psi}\rangle\Big)(A_x - \mathbf{1})\,|\widetilde{\Psi}\rangle}^{\boxed{6}}\ +\ 2\Big(\overbrace{\langle\mathcal{L}|vA_x^\dagger|\widetilde{\Psi}\rangle - 2\,\langle\mathcal{L}|v|\widetilde{\Psi}\rangle + \langle\mathcal{L}|vA_x|\widetilde{\Psi}\rangle}^{\boxed{7}}\ +\ \langle\Psi|v\Big(A_y^\dagger - 2\times\ \mathbf{1} + A_y\Big)|\widetilde{\Psi}\rangle\Big)$$
$$.$$

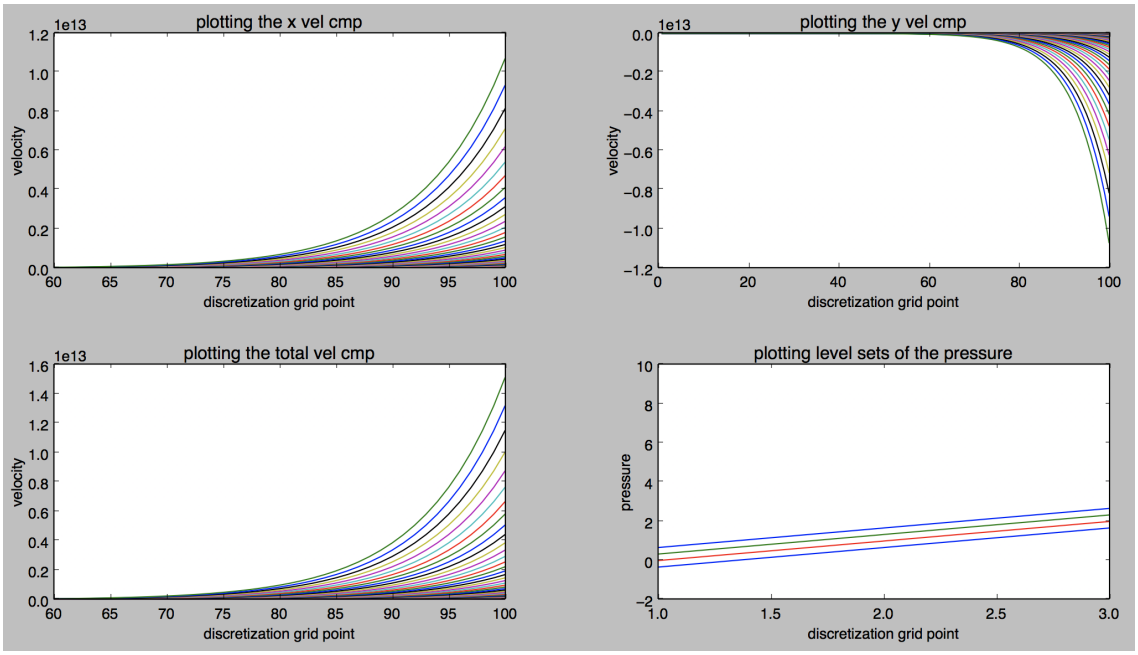

Figure 1: *For exact solutions to Navier-Stokes, the x component of the velocity satisfies $v_x = A\ \exp\Big(c/\{\nu(\alpha^2+\beta^2)\}(\alpha x + \beta y)\Big) + B$, while the y component of the velocity satisfies $v_y = 1/\beta\Big(c - \alpha B - \alpha A\ \exp\big(c/\{\nu(\alpha^2+\beta^2)\}(\alpha x + \beta y)\big)\Big)$ where $\alpha, \beta \in \boldsymbol{R}$. For α and β of agreeing sign, namely both quantities taken to be positive or negative, the individual components of the velocity, in addition to the total component of the velocity of the solution, are illustrated. A free parameter choice which strongly favors α or β, or vice versa, results in components of the solution exhibiting variable rates of exponential growth or decay in the velocity as the grid point of the discretization varies.*

2.2 Earlier studies of solutions to Navier-Stokes in the plane

Previous works have investigated several different aspects of the Navier-Stokes equations, whether it be the domain over which solutions are obtained, specific assumptions of the behavior of the pressure gradient under translations and rotations and over discretizations of varying composition [17]. In higher dimensional cases beyond the plane, past works have studied the regularity structure of solutions to the partial differential equation, as well as providing solutions for the equations driven by space time white noise through arguments relating to the construction of Gaussian invariant measures and fixed point mappings [28,29].

On the other hand, efforts have also been made to prove analytical solutions for example pressure distributions to the equations as given in [18]. By comparison with analytical solutions under assumptions on choice of parameters, comparisons between the cost function and exact solutions to the equations can be determined. Next, to observe conservation laws of the system for other quantities, whether it be helicity, 2D entrophy or total vorticity of the trajectory, Charnyi, Heister, Olshanskii and Rebholtz in [5] introduce numerical methods for simulating the pressure across three dimensional objects including a square cylinder.

With observations stemming from Riemannian geometry and connections to the behavior of the Ricci curvature and trajectory of Brownian motion, Arnaudon and Cruziero [3] make statements of the variational principle allowing for arguments inovlving the covariant derivative in which symmetry of the Ricci curvature tensor through a damped Laplacian is formalized. Relatedly, Cresson and Darses [7] provide formulations of the Navier-Stokes and Stokes equations for incompressible fluid flow, while Apte, Auroux and Rammaswamy [2] avoid finite differencing the equations to obtain solutions that are finite in time, but with unknown pressure as initial conditions, directly opposite to the procedure in [18]. *Figure 1* shows plots of solutions to Navier-Stokes for the x and y components of the velocity solution.

2.3 Organization

We present results from quantum circuits to compute all required expectation values of the cost function. Then, within the framework of the variatonal algorithm, we present behaviors of expectation terms of the cost function, to discuss overall performance of the variational algorithm.

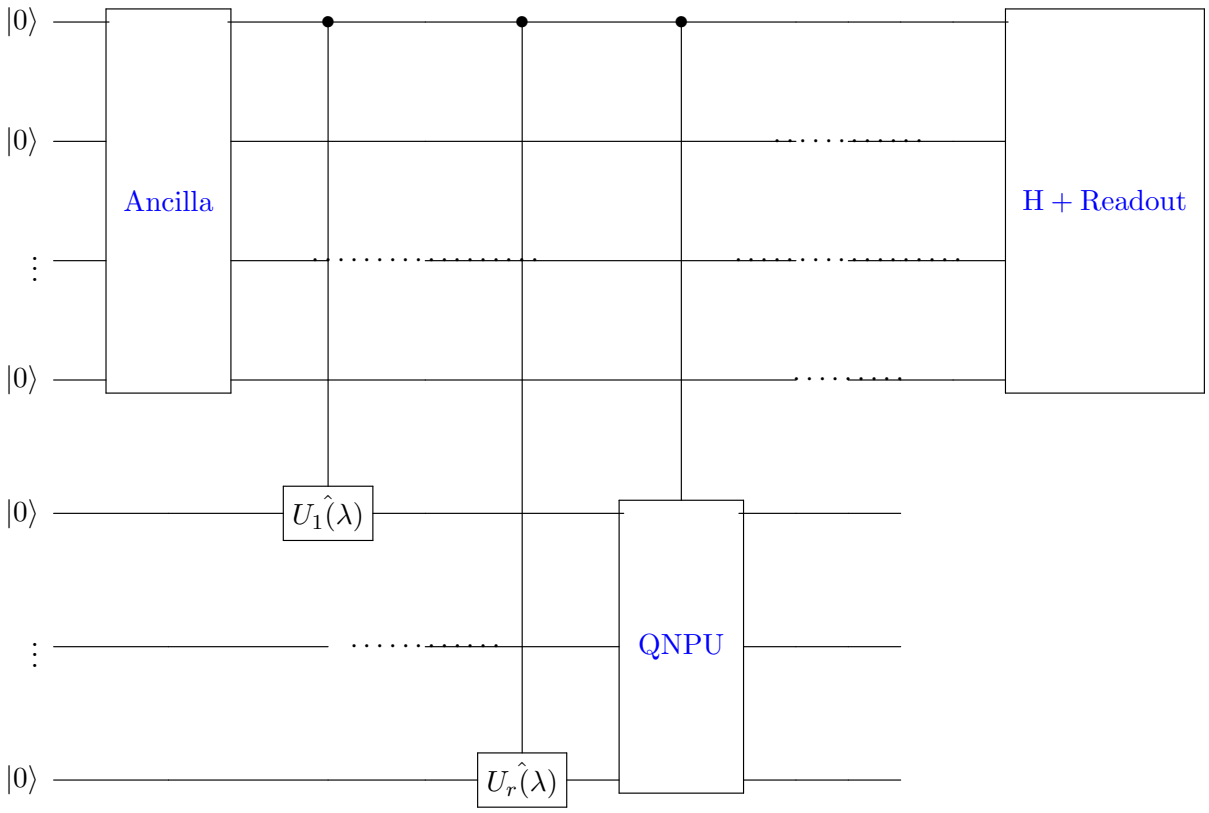

Figure 2: *Quantum circuit diagram for the Navier-Stokes variational algorithm.* With sufficient ancilla registers for carry bits associated with computation of expectation values in $\mathcal{C}$ and each prefactor, the topmost ancilla bits initialized to the 0 states undergo Hadamard gates in the Ancilla block for their first operation before being time evolved and entering the QNPU, in addition to passing through additional Hadamard operations before each read out. From previous specifications on circuit architecture, we include $n = 4$ qubits to account for the time evolution in each direction of freedom. The ancilla bits are significant for storing intermediate computations of $\mathcal{C}$, which as shown in *Figure 2*, consists of scalar addition and multiplication of quantities dependent on the Reynolds number ρ. The interaction between the control and target qubits after being fed into the QNPU is shown below in *Figure 2*. Additional terms that must be processed within the QNPU are separated based on the quantum state that must be prepared in the computed past the 0 state initialization, including the cost functions introduced in *Section 2.1*. After each ancilla is time evolved forwards, upon entry to the QNPU (below in *Figure 3*) further quantum computation is performed; for our considerations in the circuit diagram above a potential number of time evolution gates is included, but measurements in each time steps for solutions in the plane include computations of each component of the velocity, in addition to the pressure distribution at each grid point. Upon observation, the wave function for each control qubit collapses.

2.4 Acknowledgments

The author would like to thank Professor McMahon for suggesting a direction for the project. Also, many thanks to fellow team members in the McMahon Lab variational PDE subgroup, including Thomas, Leeseok, Rithesh, Yilian, Natalia & Matthew, as well as several others, for simulating discussions and thoughts.

3 Quantum circuits

3.1 Expectation computations from the cost function

Construction of the elementary circuits below demonstrates the sequence of gate operations from which the quantum-classical computational loop is executed. From foundational representations of quantum networks as a sequence of reversible unitary transformations [25], we achieve efficient computations executable through adaptations of the variational algorithm of [15] with hardware efficient algorithm which could be further test in future work for implementation on circuits with more qubits. From terms that are included in the cost function, we introduce circuits for successful quantum computation through enforcement of the number of qubits on which the algorithm will be ran, in addition to peculiar characteristics of nonlinearities of the Navier Stokes equations. In particular, the requisite circuits for the cost function revolve about quantifying the time evolution of Brownian particles under forces which respect conservation of momentum. For quantum circuit representations of expectations in the cost function, the discrete derivative operators about each planar degree of freedom require that we include circuit representations for the plain adder to process quantum computations involving the

time evolution of fluid governed by the equations.

As in [15], the subcircuits listed below will be situated within the QNPU which is necessary for the cost function minimization. To account for complexity posed by the Navier-Stokes cost function, in addition to several other computational problems, ranging from those associated with vanishing gradients of the cost function to ansatz construction [11], expressibility of parametrizations for quantum circuits [23], qubit quality, noise and complexity growth [4,10], different forms of ansatzae for the equations will be studied and qualitatively compared. In particular, for the cost function given on the previous page, we identify all 8 relevant terms and provide the circuit representations. To systematically characterize the coverage of the Hilbert space that we expect from circuit simulations, we identify each of the cross terms from the expansion of the square of the norm of the cost function that is obtained from Euler's method. With suitable circuit representations and tracing of the output, we describe more general architecture of the quantum circuits besides the adder, with implications for complexity of the algorithm and exploration of the optimization landscape.

3.2 Architecture

Before executing gates of the QNPU, to trace output of control qubits in the circuit we illustrate the number of initialized $|0\rangle$ states required for the execution of the variational algorithm from [15]. For nonlinearities of the Navier-Stokes equations, executing nonlinearities raised by the cost function for the QNPU alone requires that we include additional qubits so that the three expectation values from the cost function can be added together. Moreover, we must appropriately situate the input ports into the QNPU from previous gate operations in the circuit following the $|0\rangle$ state initialization.

To execute all relevant gate operations, we perform circuit simulations on $n =$ target qubits. We enforce this number of target qubits in the implementation because it is not only representative of degrees of freedom in the plane for which closed forms have been obtained, but also because it allows for specifications of ancilla bits that must be controlled while performing adder operations upon entry into the QNPU. More specifically, for the first target qubit initialized to $|0\rangle$, after applying the Hadamard gate and time evolving the quantum state forwards, the Navier-Stokes QNPU processes target qubits following these previous gate operations with an adder to compute the shift of all terms in the cost function. To accommodate the circuit construction so that all gates reflect the capability of the algorithm to be applied to other nonlinear equations, we incorporate standard variational parameters λ over which the cost function will be minimized. Throughout the minimization procedure, we incorporate an adder circuit to determine the summation of all terms of the cost function, requiring that we have sufficient ancilla bits for outstanding operations on the quantum computer. Specifically, the operations associated with $C(\lambda)$ include scalar multiplication computations of the variational parameter λ_0 with itself, the variational parameter $\tilde{\lambda}_0$ with $\left(\frac{\tau}{h}\right)^2$, and $\left(\frac{\tau}{\rho h}\right)^2$. Besides these terms, additional computations must be dealt with by isolating all accompanying prefactors to each expectation value, including $-\frac{\tau}{h}\lambda_0^*\tilde{\lambda}_0$, $\frac{\tau}{\rho h}\lambda_0^*$, and $-\frac{1}{\rho}\left(\frac{\tau}{h}\right)^2\tilde{\lambda}_0$, respectively. Finally, additional carry bits must be included in the control port (CP) to the QNPU so that carry bits can be established for adding the three expectation values together before the real part of the resultant is taken. In the following circuit diagram beginning with *Figure 1*, we establish all such specifications on the ancilla within the computational basis. Furthermore, the appropriate multiplication of each prefactor must correspond to a suitable number of ancilla in the CP which must be specified before the time evolution is initiated.

Specifically, in the quantum circuits for the Navier-Stokes equations, we demand that the control port contain two ancilla for operations associated with adding expectation values together. In particular, besides the topmost control qubits which undergo Hadamard gates before entering the QNPU, additional ancilla must be provided for multiplication with each prefactor previously mentioned. With the quantum Fourier Transform (QFT), quantum network representations for dividing scalars can be achieved by loading the divisor and dividend into quantum registers. This scheme is applicable to computations involving each expectation term, which after being computed individually, and multiplied by each corresponding prefactor, has a resultant term from the three values. Because the order in which the expectations are added is irrelevant, for simplicity we group together the first and third expectation values from $\mathcal{C}(\lambda, \lambda_0)$ which have the same time, to then determine contributions before taking the real part of the superposition of expectations. The circuit in *Figure 1* illustrates the circuit arrangement over which computations will be executed. The ancilla block on the topmost layer of an arbtirary number of control qubits each undergo Hadamard operations, while the topmost control qubit is responsible for time evolving each of the target qubits represented in the circuit diagram below the Ancilla block.

The remaining boxes in the circuit are responsible for the following operations. The QNPU treats nonlinearities of the Navier-Stokes equations from expectation terms in $\mathcal{C}$, while the H + Readout block applies the Hadamard gate to each ancilla after the QNPU and reads out each value after an application of $\hat{\sigma_z}$. Furthermore, it is important to quantify the number of control qubits associated with addition or multiplication on the quantum computer from the prefactors that have been previously identified. In light of rearrangements of $\mathcal{C}$ in *Section 2.1*, we present a synopsis below of the number of ancilla required in the topmost registers of the circuit from *Figure 1*; specifically, factoring out the constant from the superposition of expectation terms from the real term of $\mathcal{C}$ in ★ before further rearrangements for the cost functions for $|f(t)\rangle$ and $|p(t)\rangle$, outside of the multiplication of scalar terms, permits for one operation of multiplication after the summation of all expectation terms has been computed, to be followed by division by τ. Quantum circuit representations of integer division in [30] are achieved through dedication of ancilla to the divisor and dividends of integers in an expression,

ultimately relying on the QFT for quantum integer division. The "Clifford + T" gate family is applied to individually load divisors, dividends and remainders into the quantum circuit for computation, and in our case can simply be applied to the cost function with dividend and divisor; in the case of the Navier-Stokes cost function, the dividend itself must be loaded in as a scalar product. Outside of the QNPU, results of quantum computation for the cost function are terminated as the final read outs for the ancilla are executed from the H + Readout block.

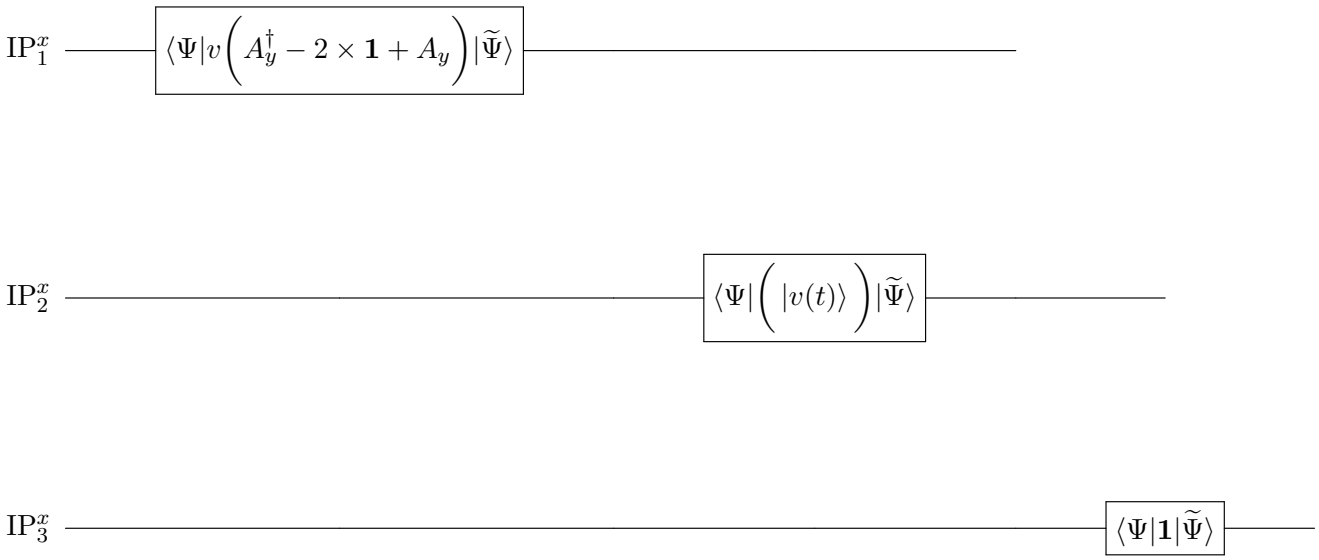

Figure 3: *QNPU circuit diagram, expectation terms from the Navier-Stokes cost function which are independent of the pressure distribution p.* Qubits in each input port to the QNPU are shown after time evolution. The ancilla bits from *Figure 1* demonstrate the portion of the circuit architecture which requires that intermediate results be stored in the quantum computer, either due to addition or scalar multiplication operations. Under the assumption of a vanishing pressure distribution discussed in *2.1.1*, expectation terms within the QNPU can be distributed as follows within the proposed Navier-Stokes circuit architecture. First, we arrange the quantum registers in the QNPU on the basis of the most significant qubits being stored in the uppermost registers of the circuit, which include the expectation terms $\langle\Psi|v\Big(A_y^\dagger - 2\times\mathbf{1} + A_y\Big)|\widetilde{\Psi}\rangle$, $\langle\Psi|\Big(|v(t)\rangle\Big)|\widetilde{\Psi}\rangle$ and $\langle\Psi|\mathbf{1}|\widetilde{\Psi}\rangle$. Second, we arrange each qubit for computation as shown above, in which the expectation term in the topmost qubit is computed by forming the quantum state resulting from the time evolution of qubits initialized to the $|0\rangle$ state below the ancilla qubits in *Figure 1.* The remaining two qubits below are computed by preparing the variational states of $|v(t)\rangle$, and computing the expectation value under the identity state $\mathbf{1}$, respectively. The portion of the QNPU architecture displayed in *Figure 4* illustrates how the first three constant terms which appear in all cost functions $\mathcal{C}$ are computed, and the states that are produced in the three registers above corresponding to pressure independent expectation terms in $\mathcal{C}^{\,0,x}$ after surpassing the prescribed gates are output from the QNPU, illustrated in the quantum registers below those of the ancilla qubits in *Figure 1.*

We collect all expectation values from terms given in the previous section. Within the broader context of the algorithm, we initially prepare all qubits in the 0 state and furthermore, examine the $\hat{U}_j(\lambda)$ gates, where j runs over the number of qubits. A subset of the expectation terms from the Navier-Stokes cost function are represented in the QNPU for one component of the solution in *Figure 3*, from which further discussion is devoted towards circuit architecture for computations involving both components of the solution.

3.3 Classical sampling

One direction of future interest for optimization the cost function when obtaining readout from the variational algorithm for Navier-Stokes centers about making use of Brownian bridge sampling, as an indication of whether the optimization procedure has encountered a plateau in the energy landscape.

By contrasting the distribution of the random samples within a fixed box B, and outside of the same box, we establish immediate connections between the short and long range interactions of the system. Through the construction of couplings $\mathcal{J}_{ij}$ for a Hamiltonian $\mathcal{H}$, the time evolution of turbulent flow is modeled under $\mathcal{H}$ by:

- forming a sample array of the bridge values that are randomly assumed within a fixed $B_{x_i}^{\epsilon}$,
- determining the displacement of the bridge sampling at each neighboring point in the array by forming the pointwise difference between neighboring elements of the array,

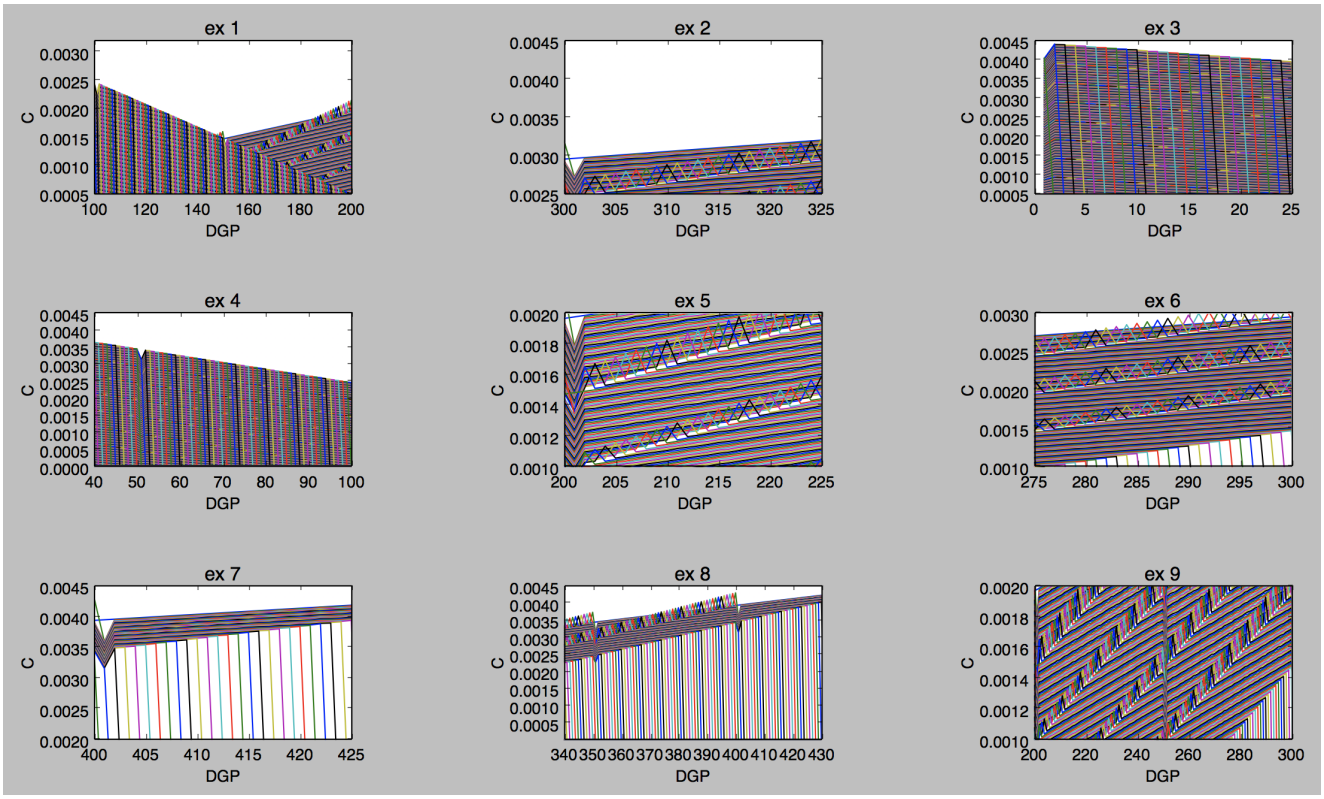

Figure 4: *Each entry in the plot above demonstrates more of the self similar, fine grained behavior in the long range couplings plot. In the first subplot, a portion of the long range couplings surface exhibits a collection of couplings for which the bridge samples are inversely proportional to the grid point that is sampled, as the number of points increases. DGP indicates the discretization grid point at which a sample is collected. In the second plot, another portion of the surface exhibits the couplings at which different curves, whether colored yellow or blue, reach a fixed maximum coupling constant which is dependent on the nature of the underlying sampling distribution. In the third plot, another perspective of the decay of the long range couplings is shown, in the yellow line which intersects the axis around the fifth discretization point sharply decays in the magnitude of its coupling as the same process proceeds to draw the fifth random variable. In the fourth plot, a similar pattern at the number of discretization point at which the yellow, and any other colored lines approach* 0 *is observed. In the fifth and sixth plots, zoom ins of the peaks of each long range coupling constant sequence from the second plot is given. In the seventh plot, the long range couplings numerically decrease in a similar manner as given in the fourth plot, but experience a sharp decay after the* 400*th discretization point. In the eighth plot, the maximum of the triangular interfaces increase montonically with the discetization point, and approach* 0 *at a later time. In the ninth plot, the portion of the long range couplings surface in between the maxima of every color line is achieved. In fact, after achieving the maxima, upon close examination one can see that the yellow lines continue to increase as the grid discetization point number increases, and then approach to* 0 *after a sufficient number of samples has been drawn.*

- constructing the couplings within $B^{\epsilon}_{x_i}$, and outside of $B^{\epsilon}_{x_i}$, which are of the form $\mathcal{J}_{ij} = \frac{|t_i - t_j|}{\sum_{\text{Box}} t_k} \exp(-|x_i - x_j|)$, intentionally defined so that the turbulent flow between points that achieve a maximum distance away from each other in $B^{\epsilon}_{x_i}$ not only decays exponentially with respect to the Euclidean distance between the point, but also so that the long and short range couplings of $\mathcal{H}$ can be formed by partitioning the sample array into the number of steps $\mathcal{N}$ taken in each box of the discretization,
- computing $\mathcal{H}$,
- comparing the probability of different configurations occurring, dependent on the random samples of the bridge from a fixed frame of reference, with the law $\mathbf{P} = \frac{\exp(-\mathcal{H})}{\mathcal{Z}}$, where $\mathcal{Z} = \sum_{\text{Box}} W(t)$, where $W(t)$ is the continuous trajectory of the bridge.

4 References

[1] Albert, V., Covey, J. & Preskill, J. Robust Encoding of a Qubit in a Molecule. *Phys Rev* **10** 031050 (2020).

[2] Apte, A., Auroux, D. & Ramaswamy, M. Observers for Compressible Navier-Stokes Equation. arXiv: 1503.05259 (2015).

[3] Arnaudon, M. & Cruzeiro, A.B. Lagrangian Navier-Stokes Diffusions of Manifolds: Variational Principle and Stability. arXiv: 1004.2176 (2010).

[4] Brandao, F. et al. Models of quantum complexity growth. arXiv: 1912.04297 (2019).

[5] Charnyi, S., Heister, T., Olshanskii, M.A. & Rebholz, L.G. On conservation laws of Navier-Stokes Galerkin discetizations. *Journal of Computational Physics* **337** 289-308 (2016).

[6] Chowdhury, A., Low, G.H. & Wiebe, N. A Variational Quantum Algorithm for Preparing Quantum Gibbs States. arXiv: 2002.00055 (2020).

[7] Cresson, J. & Darses, S. Lagrangian Structure for the Stokes, Navier-Stokes and Euler Equations. arXiv: 0811.3286 (2008).

[8] Eremenko, A. Spectral Theorems for Hermitian and Unitary Matrices. *Lecture Notes.*

[9] Faist, P. et al. Continuous symmetries and approximate quantum error correction. arXiv: 1902.07714 (2019).

[10] Gidney, C., Ekera, M. How to factor 2048 bit RSA integers in 8 hours using 20 million noisy qubits. arXiv: 1905.09749 (2019).

[11] Hadfield, S., Wang, Z., O'Gorman, B., Rieffel, E., Venturelli, D. & biswas, R. From the Quantum Approximate Optoimization Algorithm to a Quantum Alternating Operator Ansatz. *Quantum Optimization Theory, Algorithms, and Applications* **34** 12.2 (2019).

[12] Iverson, J. & Preskill. J. Coherence in logical quantum channels. *New Journal of Physics* **22** 073066 (2020).

[13] Kandala, A., et al. Harware-efficient Variational Quantum Eigensolver for Small Molecules and Quantum Magnets. *Nature* **549** 242 (2017).

[14] Kim, I., Swingle, B. Robust entanglement renormalization on a noisy quantum computer. arXiv: 1711.07500 (2017).

[15] Lubasch, M., et al. Variational quantum algorithms for nonlinear problems. *Phys Rev* **101** 010301 (2020).

[16] McClean, J.R. et al. The theory of variational hybrid quantum-classical algorithms. *New J. Phys.* **18** 023023 (2016).

[17] Nakaji, K. & Yamamoto, N. Expressibility of the alternating layered ansatz for quantum computation. arXiv: 2005.12537 (2020).

[18] Otarod, S. & Otarod, D. Analytical Solutions for Navier-Stokes Equations In Two Dimensions For Laminar Incompressible Flow. arXiv: physics/0609186v1 (2006).

[19] Orus, R. A Practical Introduction to Tensor Networks: Matrix Product States and Projected Entangled Pair States. *Annals of Physics* **349** 117-158 (2014).

[20] Perez-Garcia, D., Verstraete, F., Wolf, M.M. & Cirac, J.I. Matrix Product State Representations. *Quantum Inf. Comput.* **7** 401 (2007).

[21] Peruzzo, A., et al. A variational eigenvalue sdolver on a quantum processor. *Nature Communications* **5** 4213 (2014).

[22] Preskill. J. Quantum computing in the NISQ era and beyond. *Quantum* **2**(79) (2018).

[23] Sim, S., Johnson, P. & Aspurur-Guzik, A. Expressibility and entangling capability of parametrized quantum circuits for hybrid quantum-classical algorithms. *Advanced Quantum Technologies* **2**(12) (2019).

[24] Sung, K., et al. Using models to improve optimizers for variational quantum algorithms. *Quantum Science and Technology* **5**(4) (2020).

[25] Vedral, V., Barenco, A. & Ekert, A. Quantum Networks for Elementary Arithmetic Operations. *ArXiv*: quant-phy/9511018.

[26] Xu, X. et al. Variational algorithms for linear algebra. arXiv:1909.03898 (2019).

[27] Zhang, D.B., Zhan-Hao, Y. & Yin, T. Variational quantum eigensolvers by variance minimization. arXiv: 2006. 15781 (2020).

[28] Zhu, R. & Zhu, X. Three-dimensional Navier-Stokes equations driven by space-time white noise. arXiv: 1406.0047 (2014).

[29] Grotto, F. & Pappalettera, U. Gaussian invariant measures and stationary solutions to 2D primitive equations arXiv: 2005.03339 (2020).

[30] Thapliyal, H., Munoz-Coreas, E., Varun, T.S.S. & Humble, T.S. *Quantum Circuit Designs of Integer Division Optimizing T-count and T-depth.* arXiv:1809.09732 (2018).

[31] Zhuang, Q., Preskill, J. & Jiang, L. Distributed quantum sensing enhanced by continuous-variable error correction. *New Journal of Physics* **22** (2020).

[32] Abughalia, M.A. On the mathematical solution of the 2D Navier Stokes equations for different geometries. *Advances in Fluid Mechanics* **39** 2006.